Distortion-Aware Power Allocation for 6G MIMO Transmitters

Deepa Gunasekaran and Frank Sakalani

Department of Electrical and Information Technology
Lund University

Supervisor (Ericsson AB): Mohamed Hamid

Co-Supervisor (Ericsson AB): Bo Göransson

Supervisor (LTH): Juan Vidal Alegría

Co-Supervisor (LTH): Ashkan Sheikhi

Examiner: Ove Edfors

June 10, 2026

Abstract

Future sixth-generation (6G) wireless systems are expected to support extreme data rates, massive connectivity, and high energy efficiency. Large-scale Multiple-Input Multiple-Output (MIMO) combined with Orthogonal Frequency Division Multiplexing (OFDM) is a key enabling technology to meet these demands. However, OFDM signals exhibit a high Peak-to-Average Power Ratio (PAPR), which forces power amplifiers (PAs) to operate with significant back-off in order to satisfy Error Vector Magnitude (EVM) and spectral emission constraints, thereby reducing transmitter efficiency.

This thesis investigates distortion-aware power allocation in OFDM-based MIMO transmitters with a focus on 6G-oriented system design. The work analyzes the spatial and spectral behavior of distortion introduced by Crest Factor Reduction (CFR) and nonlinear PA characteristics. A comprehensive simulation framework is developed based on wideband CP-OFDM transmission, DFT beamforming, and multi-user MIMO to evaluate distortion under spatial, frequency, and joint spatial–frequency multiplexing.

The results reveal that branch-level distortion does not directly translate to user-experienced distortion. With increasing number of simultaneously served users, nonlinear distortion becomes progressively decorrelated from the desired signal components, resulting in significantly lower user EVM compared to branch EVM. A similar decorrelation effect is observed when users are separated in the frequency domain through sub-band allocation. Furthermore, increasing the number of antennas enhances distortion averaging, leading to improved user-side signal quality while branch-level distortion remains largely unchanged.

Building on these observations, the study introduces the concept of power overbooking, whereby additional transmit power can be allocated without violating user-level EVM constraints. The results demonstrate that joint exploitation of spatial and frequency resources provides measurable power headroom gains, enabling reduced PA back-off and improved energy

efficiency.

Overall, this work highlights that distortion-aware and hardware-aware resource allocation can significantly improve transmitter performance. The findings provide practical design insights for future large-scale MIMO systems, where exploiting distortion decorrelation across space and frequency becomes a key enabler for energy-efficient 6G transmitter architectures.

Acknowledgement

We would like to express our sincere appreciation to Ericsson for providing the opportunity to carry out this master's thesis in collaboration with Lund University. The collaboration has offered a valuable environment for applying academic knowledge to practical research challenges and has contributed significantly to our learning experience.

We would also like to extend our gratitude to the **Swedish Institute** for supporting Frank Sakalani in pursuing his Master's studies at Lund University (LTH). This support has played an important role in enabling his academic journey and the completion of this thesis.

We sincerely thank everyone at Ericsson for fostering a welcoming and supportive work environment throughout the thesis period. In particular, we are grateful to our supervisors, Mohamed Hamid and Bö Göranson, for their guidance, continuous support, and valuable technical discussions.

We also wish to thank our academic supervisors at Lund University, Juan Vidal Alegría and Ashkan Sheikhi, for their guidance, constructive feedback, and insightful discussions, which have contributed greatly to this work.

Furthermore, we would like to thank our examiner, Ove Edfors, for his valuable feedback and support during the course of this thesis.

Finally, we gratefully acknowledge the support and encouragement of our families and friends throughout our studies.

Popular Science Summary

Every time we watch a video, make a phone call, or use mobile internet, wireless signals are transmitted between our devices and nearby base stations. As society becomes increasingly connected, future mobile networks, often referred to as 6G, will need to deliver much higher data rates while consuming less energy.

One of the major challenges is that radio transmitters are not perfectly efficient. To send information over the air, transmitters use power amplifiers that boost the signal before it reaches the antenna. However, when these amplifiers are pushed too hard, they introduce distortion, which can reduce communication quality and cause interference. To avoid this problem, transmitters are often operated below their maximum power, which improves signal quality but wastes energy.

Modern wireless systems use many antennas simultaneously, a technology known as Multiple-Input Multiple-Output (MIMO). These antennas work together to direct signals toward specific users. Interestingly, distortion generated by different antennas does not always combine in the same way as the desired signal; in many situations, distortion spreads out in different directions, while the useful signal remains focused on the intended user.

This thesis investigates how this behavior can be exploited in future 6G systems. Through computer simulations, different ways of serving multiple users were studied, including separating users in space, frequency, or a combination of both. The results show that the communication quality experienced by users can often be significantly better than what is suggested by measurements taken directly at the transmitter antennas, meaning that current design rules can be overly conservative.

These findings indicate that future wireless systems may be able to operate at higher power levels than currently assumed without reducing user experience. Such distortion-aware operation could improve energy efficiency, extend coverage, and increase network capacity, contributing to greener and more efficient wireless communication technologies for future generations of mobile networks.

Table of Contents

List of Acronyms and Abbreviation

3GPP	3rd Generation Partnership Project
5G	Fifth Generation
6G	Sixth Generation
ACLR	Adjacent Channel Leakage Ratio
CFR	Crest Factor Reduction
EVM	Error Vector Magnitude
IDFT	Inverse Discrete Fourier Transform
ISAC	Integrated Sensing and Communications
LOS	Line Of Sight
MIMO	Multiple Input Multiple Output
NF	Noise Figure
NMSE	Normalized Mean-Square Error
OOB	Out-Of-Band
OFDM	Orthogonal Frequency Division Multiplexing
PA	Power Amplifier
PAPR	Peak-to-Average Power Ratio
RF	Radio Frequency
UEs	User Equipment

Chapter 1

Motivation

Orthogonal Frequency Division Multiplexing (OFDM) has been widely adopted in modern wireless communication systems, including 5G and emerging 6G systems, due to its robustness against multipath fading and its ability to mitigate inter-symbol interference (ISI) by transmitting data over multiple orthogonal subcarriers. However, despite these advantages, OFDM signals inherently suffer from a high peak-to-average power ratio (PAPR).

When OFDM signals are transformed from the frequency domain to the time domain, the superposition of multiple subcarriers results in occasional constructive alignment of signal components, producing large instantaneous power peaks. These peaks pose a significant challenge for radio-frequency power amplifiers (PAs), which are typically designed to operate efficiently near their saturation region.

To avoid nonlinear distortion caused by these peaks, a common approach is to operate the PA with input back-off (IBO), effectively reducing the average transmit power to accommodate peak excursions. However, this back-off leads to a significant degradation in power efficiency, often in the order of 10–15%, which directly impacts system capacity, coverage, and energy efficiency—key performance indicators in 5G and beyond.

An alternative approach is to apply peak reduction techniques such as Crest Factor Reduction (CFR), where the signal peaks are clipped to allow for higher average transmit power. While CFR improves power efficiency by reducing the required back-off, it introduces distortion into the signal. Conventional CFR methods are primarily designed to suppress out-of-band distortion to meet spectral emission requirements, but they leave residual in-band distortion, which degrades the error vector magnitude (EVM) at the transmitter branches.

In legacy systems, the primary design criterion has been to meet branch-level EVM constraints without fully exploiting the spatial domain properties of multi-antenna (MIMO) systems. This raises a key research question: whether it is possible to allow more aggressive clipping at the transmitter, intentionally introducing controlled distortion that can be spatially shaped or distributed such that it minimally impacts the end-user EVM.

This thesis is motivated by the hypothesis that, in multi-antenna systems, distortion can be steered or projected into less harmful spatial directions, thereby relaxing traditional constraints on per-branch EVM. Such distortion-aware power allocation strategies could enable operation closer to saturation, reducing the need for back-off while maintaining acceptable user-level performance.

The central objective is, therefore, to investigate how much additional transmit power can be extracted beyond conventional back-off limits (power overbooked) while ensuring compliance with system-level performance metrics. This involves analyzing the trade-off between clipping-induced distortion, spatial processing, and achievable gains in power efficiency, with the aim of improving overall system performance in future 6G MIMO transmitters.

Chapter 2

Introduction

2.1 Background

Modern wireless systems such as 4G LTE, 5G NR, and the upcoming 6G networks rely heavily on Orthogonal Frequency Division Multiplexing (OFDM) and Multiple-Input Multiple-Output (MIMO) technologies to achieve high spectral efficiency and spatial multiplexing gains [1], pp. 1–2, [2]. However, these techniques also impose strict requirements on power amplifier (PA) linearity and overall energy efficiency [3], [12], [5]. Due to the inherently high peak-to-average power ratio (PAPR) of OFDM signals, power amplifiers must operate within their linear region to meet Error Vector Magnitude (EVM) and out-of-band emission limits [3], . This constraint often leads to significant power back-off, resulting in reduced power efficiency [5], [6]. To mitigate the effects of non-linearity, techniques like Digital Pre-Distortion (DPD) and Crest Factor Reduction (CFR) are commonly employed, but these solutions introduce their own trade-offs between distortion and efficiency [3], [8], [5]. In Massive MIMO (M-MIMO) and multi-user MIMO (MU-MIMO) systems, transmit power varies across antenna branches because of precoding, user scheduling, and resource allocation [5], [6]. Consequently, EVM and clipping distortion differ across branches and layers, affecting the achievable SNR and link throughput [5], [6]. Future systems, therefore, need distortion-aware power allocation strategies that can anticipate these effects during scheduling and link adaptation [3], [12], [5], [6]. These observations highlight the need for distortion-aware power allocation and scheduling approaches that explicitly account for hardware limitations. As wireless systems evolve towards 6G, where energy efficiency, scalability, and hardware-awareness play an increasingly important role, incorporating nonlinear amplifier behavior into resource allocation becomes essential for achieving reliable and efficient transmission.

2.2 Thesis contribution

This thesis is expected to contribute to the design of **power-efficient and distortion-aware OFDM-based MIMO transmitters** by addressing the fundamental inefficiencies introduced by high peak-to-average power ratio (PAPR) in power amplifier (PA) in modern wireless systems. While OFDM enables robust high data-rate transmission and resilience to multipath fading, its inherent peak fluctuations require significant input back-off (IBO) to avoid nonlinear distortion, resulting in reduced energy efficiency and underutilization of available transmit power.

Conventional mitigation techniques, such as Crest Factor Reduction (CFR), enable operation at higher average power levels by introducing controlled clipping [7]. However, these methods are typically constrained by **branch-level error vector magnitude (EVM)** requirements, which do not fully capture how distortion propagates in multi-antenna transmission systems. In practical multi-user MIMO scenarios, precoding and beamforming introduce branch-dependent power variations, and emerging evidence suggests that nonlinear distortion exhibits **structured spatial and spectral characteristics** rather than behaving as purely random noise.

Motivated by these observations, this thesis aims to develop a **distortion-aware analytical and system-level framework** that better relates transmitter impairments to user-perceived performance. In particular, the work investigates whether the distortion introduced by more aggressive peak reduction can be **spatially redistributed, decorrelated, or projected into less harmful directions**, thereby minimizing its impact on end-user EVM.

Through a systematic analysis of the interplay between **clipping-induced distortion, spatial processing, and multi-user multiplexing strategies**, the thesis seeks to quantify the extent to which additional transmit power can be utilized beyond conventional back-off limits (power overbooking). The expected contribution is to establish a more realistic and unified design perspective, enabling transmitters to operate closer to saturation while maintaining acceptable communication quality.

Ultimately, this work contributes toward **hardware-aware and energy-efficient transmitter optimization**, providing a foundation for future distortion-aware power allocation and scheduling strategies in 5G-Advanced and 6G MIMO systems.

2.3 Related works and research gap

Björnson *et al.* [9] studied massive MIMO systems with non-ideal hardware. They used additive distortion noise models to find limits on energy efficiency, channel estimation, and system capacity. Their analysis is useful but mainly focuses on large-system behavior. It does not provide enough detail on dynamic power allocation per antenna branch, especially under OFDM PAPR changes and specific EVM limits.

Demir and Björnson [10] explained the Bussgang decomposition for nonlinear systems and extended it to MIMO. This approach helps model distortion in a statistical way. However, the work is mostly theoretical. It does not fully combine distortion modeling with real-time decisions on precoding, user scheduling, power overbooking, or adaptive allocation to keep EVM below 3.5% in real OFDM systems.

Mollén *et al.* investigated the spatial characteristics of nonlinear distortion in large antenna arrays, with a particular focus on **out-of-band (OOB) radiation** in massive MIMO systems. Their work showed that, unlike in legacy single-antenna systems, distortion generated by nonlinear hardware in large arrays does not necessarily follow the same beamforming pattern as the desired in-band signal. In multi-user scenarios, the OOB distortion was observed to become increasingly **spatially distributed and close to isotropic** as the number of users or spatial components increases, due to the superposition of multiple independent signals across antennas [14].

This insight has important implications for hardware design, as it suggests that linearity requirements can be relaxed without increasing interference to external systems. However, the analysis in this work is primarily limited to **out-of-band emissions and their impact on adjacent-channel interference**, and does not extend to the behavior of **in-band distortion**, which directly affects user-level performance through metrics such as EVM. As a result, the question of how distortion spreads and combines within the useful signal band, particularly in multi-user MIMO transmission, remains insufficiently explored.

Marwaha et al. [12] presented optimal power allocation methods that consider PA distortion in downlink massive MIMO-OFDM systems with zero-forcing precoding. Their work shows improvements in sum-rate, but it focuses mainly on allocation under simple assumptions. It does not fully study power overbooking or the effects of branch-dependent variations and scheduling on PAPR in large antenna arrays. Liu et al. [6] developed distortion-aware power allocation for multi-stream distributed massive MIMO with nonlinear PAs. This work helps with per-stream optimization, but it is designed for distributed systems. It offers less insight into centralized massive MIMO, especially regarding the joint effects of precoding and scheduling on PAPR or strict 3GPP EVM targets.

2.4 Research objectives and Contributions

This thesis aimed to investigate distortion-aware power allocation in OFDM-based MIMO systems, focusing on the impact of high PAPR, power amplifier non-linearity, and branch-dependent power variations in 5G and future 6G networks. It modeled how pre-coding and scheduling affect PAPR, EVM, and distortion across antenna branches, and develops power overbooking and allocation strategies that improve energy efficiency while meeting EVM and emission constraints, enabling more robust and efficient link adaptation in large-scale MIMO systems.

Chapter 3

System Overview

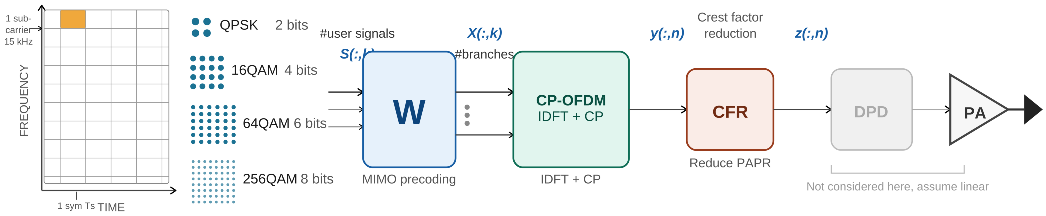

Figure 3.1: OFDM-MIMO Transmitter

The base station is equipped with a large number of antenna branches, denoted by N, serving L single-antenna user equipments (UEs), where $L \ll N$. The system employs cyclic prefix orthogonal frequency-division multiplexing (CP-OFDM) modulation to combat frequency-selective fading. Precoding is performed in the frequency domain before the inverse discrete Fourier transform (IDFT).

3.1 OFDM Signal Model

Let $\mathbf{S} \in \mathbb{C}^{M \times K}$ denote the frequency-domain data matrix, where M is the number of subcarriers and K is the number of spatial beams. The k-th column of $\mathbf{S}$, denoted $\mathbf{s}_k$, contains the QAM symbols assigned to beam k. The discrete-time baseband OFDM waveform for beam k is generated by the normalized IDFT:

$$x_k(n) = \frac{1}{\sqrt{M}} \sum_{m=0}^{M-1} S(m,k)\, e^{j2\pi mn/M}, \quad n = 0, 1, \ldots, M-1 \tag{3.1}$$

The MIMO precoding with the DFT beamforming matrix $\mathbf{W} \in \mathbb{C}^{N\times K}$ is applied to the per-beam time-domain signals (equivalent to per-subcarrier precoding in the frequency domain, since $\mathbf{W}$ is frequency-flat). The composite CP-extended signal at the antenna branch ℓ is therefore:

$$y_\ell(n) = \sum_{k=1}^{K} w_{\ell k}\, x_k(n), \quad n = -N_{\mathrm{CP}}, \ldots, M-1 \tag{3.2}$$

where $w_{\ell k}$ is the (ℓ, k)-th element of the DFT precoder matrix $\mathbf{W}$ and N_{CP} is the cyclic prefix length.

The PAPR of the signal at the antenna branch ℓ is defined as

$$\mathrm{PAPR}_\ell = \frac{\max_n |y_\ell(n)|^2}{\mathbb{E}[|y_\ell(n)|^2]} \tag{3.3}$$

High PAPR arises from the coherent addition of M independent subcarrier contributions, which can produce large instantaneous amplitude peaks. For M subcarriers with independent complex Gaussian-distributed amplitudes, the PAPR distribution is characterized by the Complementary Cumulative Distribution Function (CCDF):

$$\Pr(\mathrm{PAPR} > \gamma) \approx 1 - (1 - e^{-\gamma})^M \tag{3.4}$$

3.2 DFT Beamforming Precoder

A Uniform Linear Array (ULA) with N half-wavelength-spaced antenna elements is considered. The array steering vector for a user at an azimuth angle θ is:

$$\mathbf{a}(\theta) = \frac{1}{\sqrt{N}} \left[1, e^{j\pi\sin(\theta)}, e^{j2\pi\sin(\theta)}, \ldots, e^{j(N-1)\pi\sin(\theta)}\right]^T \in \mathbb{C}^{N\times 1} \tag{3.5}$$

The DFT beamforming matrix $\mathbf{W}$ is formed by stacking K steering vectors as columns, each corresponding to one of the K user azimuth angles $\{\theta_1, \theta_2, \ldots, \theta_K\}$:

$$\mathbf{W} = [\mathbf{a}(\theta_1), \mathbf{a}(\theta_2), \ldots, \mathbf{a}(\theta_K)] \in \mathbb{C}^{N\times K} \tag{3.6}$$

Under DFT beamforming, the normalized array radiation pattern in the spatial direction ϕ is evaluated as:

$$P(\phi) = 10\log_{10}\left(|\mathbf{W}^H\mathbf{a}(\phi)|^2\right) - 10\log_{10}(\max_{\phi}|\mathbf{W}^H\mathbf{a}(\phi)|^2) \quad [\text{dBc}] \tag{3.7}$$

Two pattern components are distinguished: the signal pattern $P_s(\phi)$ and the distortion pattern $P_d(\phi)$ arising from CFR in-band noise. The signal-to-distortion ratio in a given angular direction captures the quality of beam isolation.

When K beams are simultaneously active, the effective signal at antenna branch ℓ is formed by the superposition of all spatial streams. Reliable multi-stream reception relies on the orthogonality of the corresponding steering vectors. In practice, for sufficiently large antenna arrays, the steering vectors become approximately orthogonal, i.e.,

$$\left|\mathbf{a}^H(\theta_k)\mathbf{a}(\theta_j)\right| \ll 1, \quad k \neq j, \tag{3.8}$$

with the degree of orthogonality improving as the number of antennas N increases. This enhanced angular resolution reduces inter-beam interference, which is particularly critical for maintaining low EVM under high-order modulation schemes.

In this work, a DFT-based beamforming structure is adopted primarily for its simplicity and implementation efficiency. More importantly, it provides a well-defined and deterministic baseline that avoids introducing additional effects from advanced precoding schemes. The objective of this study is not to analyse the contribution of the precoder to EVM or power overbooking, but rather to isolate and characterise the distortion behavior introduced by the CFR process. By employing a simple DFT-based beamformer, the analysis focuses exclusively on the interaction between distortion, spatial multiplexing, and frequency-domain allocation, without confounding influences from adaptive or channel-dependent precoding.

3.3 EVM Definition

The Error Vector Magnitude (EVM) quantifies the normalized deviation between the ideal and received constellation points. For a block of L symbols transmitted on beam k, the RMS EVM is defined as

$$\text{EVM}_k = \sqrt{\frac{\sum_{\ell=1}^{L}|r_k[\ell] - s_k[\ell]|^2}{\sum_{\ell=1}^{L}|s_k[\ell]|^2}} \times 100\%. \tag{3.9}$$

Here, $s_k[\ell]$ denotes the ideal transmitted symbol on beam k at time index ℓ, and $r_k[\ell]$ denotes the corresponding received symbol after spatial combining, obtained as

$$r_k[\ell] = \mathbf{a}^H(\theta_k)\,\mathbf{y}[\ell], \tag{3.10}$$

where $\mathbf{y}[\ell] \in \mathbb{C}^N$ is the received signal vector across the N antenna elements, and $\mathbf{a}(\theta_k)$ is the steering vector corresponding to beam k. This operation corresponds to matched filtering (or inverse beamforming) for the desired user.

Two EVM metrics are tracked throughout this work:

- *Beam (user) EVM*: the EVM evaluated using $r_k[\ell]$, reflecting the signal quality at the intended receiver after spatial processing.
- *Branch EVM*: the EVM computed directly at antenna branch ℓ prior to spatial combining, capturing the distortion level at the transmitter output and serving as the constraint for power overbooking.

The EVM requirement for 256-QAM under 3GPP NR specifications is

$$\epsilon \mathrm{EVM}_{\mathrm{limit}} = 3.5\%. \tag{3.11}$$

In this work, three representative EVM targets are considered:

$$\epsilon \in \{1.8\%,\, 3\%,\, 6\%\}, \tag{3.12}$$

corresponding to different modulation orders and system operating conditions.

3.4 Power Overbooking Definition

Power overbooking characterizes the additional transmit power margin that can be exploited when the distortion constraint is governed by the per-branch EVM rather than the per-beam EVM. Let

$$\varepsilon \mathrm{EVM}_{\mathrm{limit}} \tag{3.13}$$

denote the maximum allowable EVM.

In the CFR process, the Peak-to-Average Power Ratio (PAPR) operating point is controlled through the clipping threshold, which introduces a trade-off between PAPR reduction and distortion. Let γ denote the resulting PAPR level after CFR processing. Since stronger clipping (lower γ) increases nonlinear distortion, the EVM can be expressed as a function of γ, i.e.,

$$\mathrm{EVM}_{(\cdot)} = \mathrm{EVM}_{(\cdot)}(\gamma), \tag{3.14}$$

where $(\cdot) \in \{\text{branch, beam}\}$.

Define the PAPR thresholds corresponding to a given EVM constraint as the minimum PAPR values for which the respective EVM metrics satisfy ε:

$$\mathrm{PAPR}_{\mathrm{branch}}^{(\varepsilon)} = \inf \left\{ \gamma \in \mathbb{R}_+ : \mathrm{EVM}_{\mathrm{branch}}(\gamma) \leq \varepsilon \right\}, (3.15)$$

$$\mathrm{PAPR}_{\mathrm{beam}}^{(\varepsilon)} = \inf \left\{ \gamma \in \mathbb{R}_+ : \mathrm{EVM}_{\mathrm{beam}}(\gamma) \leq \varepsilon \right\}. \tag{3.16}$$

The power overbooking margin is then defined as

$$\Omega = \mathrm{PAPR}_{\mathrm{branch}}^{(\varepsilon)} - \mathrm{PAPR}_{\mathrm{beam}}^{(\varepsilon)} \quad [\mathrm{dB}]. \tag{3.17}$$

A positive value of Ω indicates that the transmitter can operate at a higher PAPR while still satisfying the branch-level EVM constraint. This implies that the power amplifier (PA) can be driven closer to saturation than what would be inferred from beam-level EVM considerations alone.

Consequently, power overbooking enables an effective increase in transmitted power, leading to improved link budget, enhanced coverage, or higher achievable data rates in Massive MIMO–OFDM systems.

3.5 CFR Algorithm Design

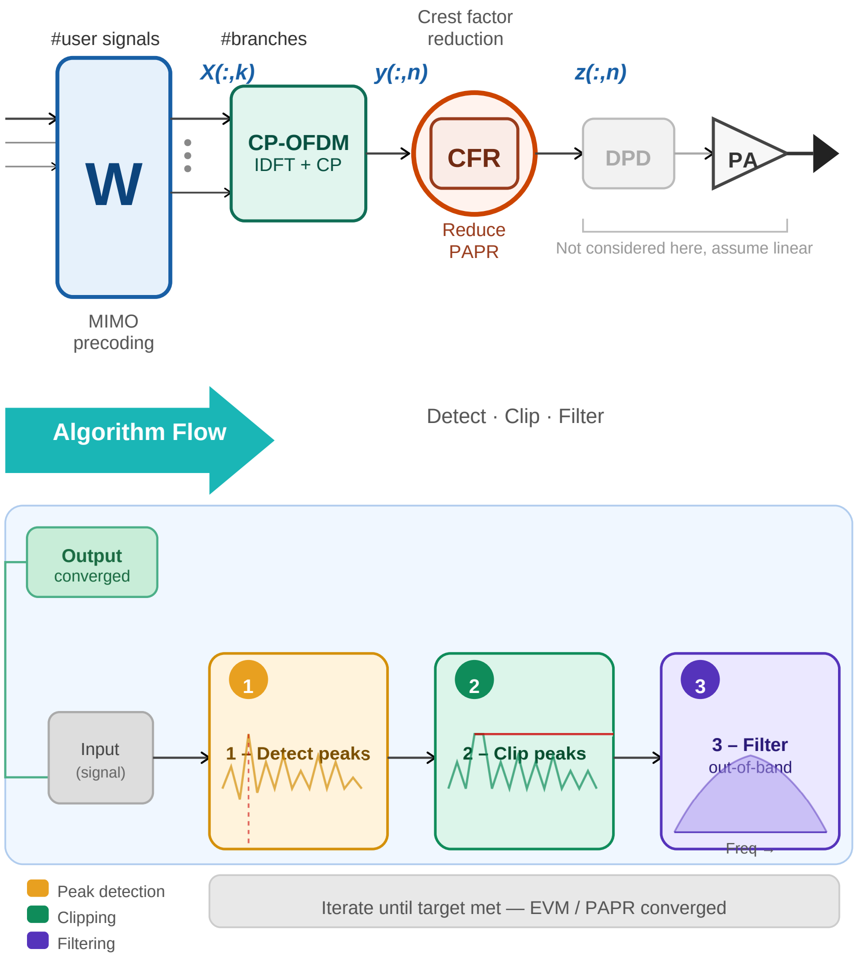

Figure 3.2: Shows the CFR algorithm

3.5.1 Algorithm Formulation

The Clipping-and-Noise Filtering (CnF) crest factor reduction algorithm operates iteratively on the discrete-time baseband signal $y[n]$ at each antenna branch. For a target peak-to-average power ratio $\mathrm{PAPR}_{\mathrm{target}}$, the clipping threshold is defined as

$$A_{\mathrm{th}} = \sqrt{\mathrm{PAPR}_{\mathrm{target}} \cdot P_{\mathrm{avg}}}, \tag{3.18}$$

where $P_{\mathrm{avg}} = \mathbb{E}[|y[n]|^2]$.

At each iteration i, the algorithm consists of four sequential steps:

1) Peak Detection and Clipping

Signal samples exceeding the threshold are identified and clipped. The clipped signal is given by

$$\tilde{y}^{(i)}[n] = \mathrm{clip}(y^{(i)}[n], A_{\mathrm{th}}), \tag{3.19}$$

where the clipping operator is defined as

$$\mathrm{clip}(y[n], A) = \begin{cases} y[n], & |y[n]| \leq A, \\ A \cdot \dfrac{y[n]}{|y[n]|}, & |y[n]| > A. \end{cases} \tag{3.20}$$

2) Clipping Noise Extraction

The clipping distortion component is obtained as

$$c^{(i)}[n] = y^{(i)}[n] - \tilde{y}^{(i)}[n]. \tag{3.21}$$

This represents the nonlinear distortion introduced by clipping, containing both in-band and out-of-band components.

3) Distortion Filtering

To suppress out-of-band emissions, the clipping noise is band-limited through a linear filter H_f with impulse response $h_f[n]$:

$$c_f^{(i)}[n] = h_f[n] * c^{(i)}[n], \tag{3.22}$$

where $*$ denotes convolution.

4) Signal Update

The filtered distortion is scaled and subtracted from the signal:

$$y^{(i+1)}[n] = y^{(i)}[n] - \alpha^{(i)} c_f^{(i)}[n], \quad 0 < \alpha^{(i)} \leq 1, \tag{3.23}$$

where $\alpha^{(i)}$ controls convergence.

The initialization is given by $y^{(0)}[n] = y[n]$, and after I iterations, the CFR output becomes

$$z[n] = y^{(I)}[n]. \tag{3.24}$$

Table 3.1: PAPR and EVM evolution versus CFR iteration index, illustrating convergence and trade-off behavior.

Iteration	PAPR (dB)	EVM (%)	Status	Remarks
1	9.20	0.4		Initial reduction
2	7.80	0.9		Large improvement
3	7.20	1.3		Diminishing returns
4	7.05	1.7	✓	Optimal (ΔPAPR < 0.02 dB)
5	7.03	2.1		Negligible PAPR gain
6	7.02	2.5		EVM accumulates

3.5.2 CFR Convergence Behavior

The results in Table 3.1 demonstrate the convergence behavior of the iterative CFR algorithm. A significant reduction in PAPR is observed during the first two iterations, followed by progressively smaller improvements in subsequent iterations toward the target PAPR of 7.0 dB. From the fourth iteration onward, the algorithm effectively converges to this target, with $\text{PAPR}^{(4)} \approx 7.05$ dB and negligible further improvement (ΔPAPR < 0.02 dB). Beyond this point, additional iterations provide minimal PAPR reduction while the EVM continues to increase due to accumulated in-band distortion. Furthermore, increasing the number of iterations leads to higher computational complexity and processing overhead in the transmitter chain. This highlights the inherent trade-off between PAPR reduction, signal quality degradation, and implementation complexity, and establishes $I = 4$ as a near-optimal operating point for the CFR design.

3.5.3 Distortion Decomposition

The CFR output signal $z[n]$ contains two distortion components. The in-band distortion $d_{\text{IB}}[n]$ falls within the transmission band and directly degrades the received constellation, thereby affecting EVM. The out-of-band component $d_{\text{OOB}}[n]$ contributes to spectral regrowth and impacts the adjacent channel leakage ratio (ACLR). The band-limiting filter H_f attenuates $d_{\text{OOB}}[n]$, although it cannot eliminate it entirely:

$$z[n] = y[n] - d_{\text{IB}}[n] - d_{\text{OOB}}[n]. \tag{3.25}$$

In the spatial multiplexing context, $d_{\text{IB}}[n]$ is the dominant impairment. When multiple beams are transmitted with approximately orthogonal steering vectors, the in-band distortion is spatially distributed. Each beam captures only a fraction of the total distortion depending on its spatial overlap with the (approximately isotropic) distortion field.

The per-beam distortion power can be approximated as

$$P_{\mathrm{dist},k} \approx \frac{P_{\mathrm{dist,total}}}{K}, \tag{3.26}$$

for K simultaneously active beams.

This spatial distortion-spreading mechanism is fundamental to Massive MIMO systems, as it reduces per-beam EVM, thereby enabling operation at higher transmit power levels and supporting higher-order modulation schemes.

Chapter 4

Simulation Setup

The simulations consider a wideband CP-OFDM downlink transmitter with multi-user MIMO beamforming. DFT-based beamforming with normalized steering vectors is applied at the transmitter. The number of simultaneously scheduled users is varied to study spatial loading, whereas the antenna array size is varied to investigate its impact on distortion projection and power overbooking.

Parameter	Value
Channel bandwidth	100 MHz
Subcarrier spacing	30 kHz
FFT size	4096
Number of PRBs	272
OFDM symbols	1
Modulation	256-QAM
Beamforming	DFT beamforming / normalized steering vectors
Users / beams	2-10
Array sizes	$N = 16, 64, 256$
EVM targets	1.8%, 3%, 6%

Table 4.1: Simulation parameters used to evaluate the distortion-aware power allocation framework.

Three user allocation strategies are considered: frequency multiplexing, spatial multiplexing, and joint spatial–frequency multiplexing. These strategies shape the time-domain waveform on each antenna branch and therefore influence PAPR, clipping noise, and EVM.

4.1 Spatial Multiplexing

In spatial multiplexing, users share the same frequency resources but are separated in the angular domain by beamforming. A uniform linear array (ULA) with half-wavelength element spacing is assumed. For each user angle, a normalized steering vector is generated and used as the beamforming weight, and different user-angle combinations lead to different overlaps between the desired beams and the associated distortion components.

To realize spatial separation in a structured way, a DFT-based beamforming grid is used. For a ULA with N antennas and inter-element spacing $d = \lambda/2$, the spatial frequency variable is defined as $u = \sin(\theta)$, and N candidate beam directions are placed on a uniform grid.

$$u_k = -1 + \frac{2k}{N}, \quad k = 0, \ldots, N-1.$$

The corresponding normalized steering vector for the k-th beam is $\mathrm{w}_{k,\ell} = \frac{1}{\sqrt{N}}\, e^{-j\pi\ell u_k}, \quad \ell = 0, \ldots, N-1.$

For a uniform linear array (ULA) with half-wavelength spacing, the angular resolution of the beamformer improves approximately inversely with the number of antennas N. Around broadside, the effective angular spacing between adjacent beams can be approximated as

$$\Delta\theta \approx \frac{2}{N} \text{ rad},$$

so that for $N = 16, 64, 256$ the corresponding resolutions are roughly 0.125 rad, 0.031 rad, and 0.008 rad, respectively. This illustrates how increasing the array size leads to finer angular resolution and more selective beam patterns.

4.2 Frequency Multiplexing

In frequency multiplexing, users are separated in the frequency domain by assigning disjoint sub-bands within the same wideband carrier. In the full-band case, all scheduled users occupy the entire active bandwidth, whereas in the sub-band case, the total bandwidth is partitioned into smaller contiguous allocations that can be assigned to different users or user groups.

The choice between full-band and sub-band allocation has a direct impact on the time-domain waveform. When users are confined to distinct sub-bands, the resulting signals on each antenna branch exhibit more localized spectral occupancy and can lead to a partial decorrelation of clipping noise between users. This can make CFR constraints less restrictive and improve the resulting EVM performance, especially when several sub-bands are active simultaneously. In contrast, full-band allocation tends to produce more strongly correlated distortion across users.

4.3 Joint Spatial and Frequency Multiplexing

4.3.1 Combined Distortion Reduction

The joint spatial and Frequency multiplexing strategy exploits both spatial beam separation and frequency-domain sub-banding to mitigate CFR-induced distortion. By combining these two mechanisms, distortion reduction is achieved across both angular and spectral domains.

Under spatial multiplexing, the transmitted beams can be designed to be orthogonal (e.g., using a DFT beamforming structure), ensuring no mutual interference at the transmitter. However, the effective steering vectors experienced by users depend on their physical angular positions and may not coincide exactly with the predefined beam directions. As a result, the steering vectors corresponding to different users are not strictly orthogonal in general.

For sufficiently large antenna arrays, the steering vectors become approximately orthogonal due to increased angular resolution, i.e.,

$$\left|\mathbf{a}^H(\theta_k)\mathbf{a}(\theta_j)\right| \ll 1, \quad k \neq j, \tag{4.1}$$

with the degree of orthogonality improving as the array size N increases. This asymptotic orthogonality reduces inter-beam interference and enables reliable multi-stream transmission.

Under this condition, the in-band distortion power is effectively distributed across the angular domain, and the per-beam distortion scales approximately as

$$P_{\text{dist},k} \approx \frac{P_{\text{dist,tot}}}{K}. \tag{4.2}$$

In logarithmic scale, this corresponds to a reduction of

$$10\log_{10}(K)\,\text{dB}, \tag{4.3}$$

reflecting the spatial spreading of distortion across K beams.

In parallel, sub-band allocation ensures that each beam is assigned a disjoint subset of subcarriers $\mathcal{B}_k$, such that

$$\mathcal{B}_k \cap \mathcal{B}_j = \emptyset, \quad k \neq j, \tag{4.4}$$

thereby achieving orthogonality in the frequency domain.

As a result, cross-beam spectral coupling of clipping noise is eliminated, i.e.,

$$P_{\text{cross}}(k \to j) \approx 0, \quad k \neq j, \tag{4.5}$$

which decorrelates distortion across beams and prevents inter-beam interference in the frequency domain.

The combined effect of spatial spreading and spectral isolation leads to compound distortion suppression. The resulting per-beam distortion can be expressed as

$$P_{\text{dist},k}^{(\text{joint})} \approx \frac{P_{\text{dist,tot}}}{K} \cdot \eta_{\text{freq}}, \tag{4.6}$$

where $\eta_{\text{freq}} \leq 1$ captures the additional distortion suppression due to sub-banding.

Equivalently, the total distortion reduction in the logarithmic domain can be approximated as

$$\Delta_{\text{dist}}^{(\text{joint})} \approx 10 \log_{10}(K) + \Delta_{\text{freq}} \ [\text{dB}], \tag{4.7}$$

where Δ_{freq} denotes the gain due to frequency-domain isolation.

This joint spatial–frequency distortion reduction directly translates into an increased power overbooking margin Ω, as validated across the parameter space $\{K, N, \varepsilon\}$. In particular, increasing the number of beams K and the array size N enhances spatial orthogonality, while sub-band allocation ensures distortion isolation, collectively enabling significant gains in achievable transmit power under a fixed EVM constraint.

Chapter 5

Results and Analysis

The simulation results for the three user allocation strategies: spatial multiplexing, frequency multiplexing, and joint spatial–frequency multiplexing. For each strategy, the key performance metrics — PAPR, branch EVM, and user EVM — are analyzed under varying conditions such as number of users, antenna array size, user geometry, and power overbooking.

5.1 Spatial Multiplexing

This section presents the results for spatial multiplexing, where all scheduled users share the same time–frequency resources and are separated purely in the angular domain by DFT beamforming. The analysis focuses on how the spatial distribution of CFR-induced in–band distortion relates to the user beams, and how this correlation or de-correlation translates into the observed branch and user EVM values.

5.1.1 DFT Beamforming Validation

The DFT beamforming implementation was validated by inspecting the antenna radiation patterns. The simulated patterns confirmed that energy is steered correctly toward the intended user angles, with main lobes aligning with the prescribed steering vectors and sidelobes suppressed in other directions.

This confirms that the beamforming weights — normalized DFT steering vectors — produce the expected spatial selectivity and that subsequent EVM results can be attributed to distortion effects rather than beamforming inaccuracies.

5.1.2 Single User Performance

To establish a baseline, a single user was scheduled at a fixed azimuth angle (here $\theta = 30°$) while all subcarriers within the active bandwidth were allocated to this user. Figure 4.1 illustrates the resulting signal and distortion patterns for $N = 64$ antennas, together with the corresponding EVM values. In this case, the branch EVM was found to be 2.55%, whereas the beam EVM seen at the user after receive combining was about 2.54%.

The nearly identical branch and beam EVM values indicate that, for a single user with a well-focused beam, the distortion pattern is strongly correlated with the user beam. In this regime the distortion adds coherently in the same direction as the desired signal and behaves mainly as an effective SNR degradation for the user.

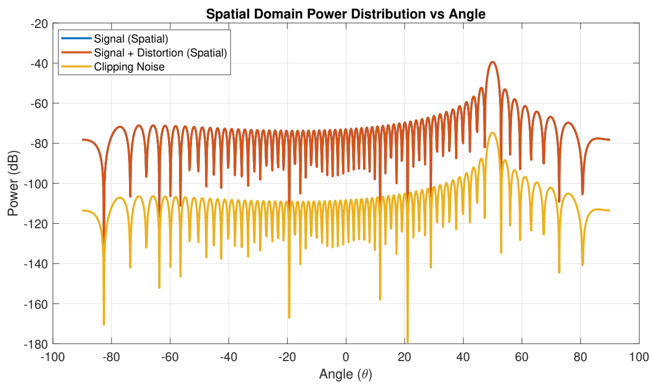

Figure 5.1: Single-user spatial multiplexing with $N = 64$ antennas. The upper curve shows the mainlobe and sidelobes of the desired signal, while the lower curve corresponds to CFR-induced in-band distortion. The EVM for branch 64 is approximately 2.553% and the user EVM is 2.541%.

5.1.3 Effect of User Geometry

Next, two users were scheduled simultaneously to study how their relative angular separation affects distortion projection. In the first scenario, the users were placed at symmetric angles $\theta_1 = -30°$ and $\theta_2 = 30°$ on the DFT grid. The corresponding radiation patterns and EVM values are shown in Figure 4.2. At the considered operating point, the worst-branch EVM is about 2.58%, while the EVMs at the two users are 2.57% and 2.57%, respectively.

With this relatively large angular separation, the beams are nearly orthogonal, and the distortion components remain well aligned with each user's signal direction. As a result, the distortion field is still highly correlated with the user beams, and the user EVMs are close to the branch EVM.

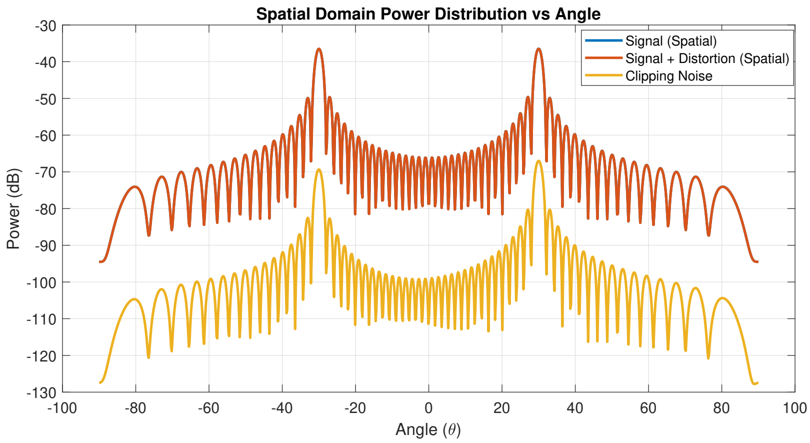

Figure 5.2: Two-user spatial multiplexing with users at $\theta_1 = -30°$ and $\theta_2 = 30°$. The reported EVMs are approximately 2.579% for the worst branch and 2.569% / 2.565% for users 1 and 2, respectively.

In a second scenario, the users were moved closer together, for example, to $\theta_1 = -50°$ and $\theta_2 = 50°$. The resulting patterns in Figure 4.3 show stronger overlap between the two main lobes and a different distribution of distortion across the array. Interestingly, at the same nominal transmit power and CFR setting, the user EVMs improve to approximately 2.19% and 2.19%. In this case the distortion energy spreads over a wider range of angles and becomes less correlated with each user beam, so that a significant part of the distortion is projected outside the effective channels of the users.

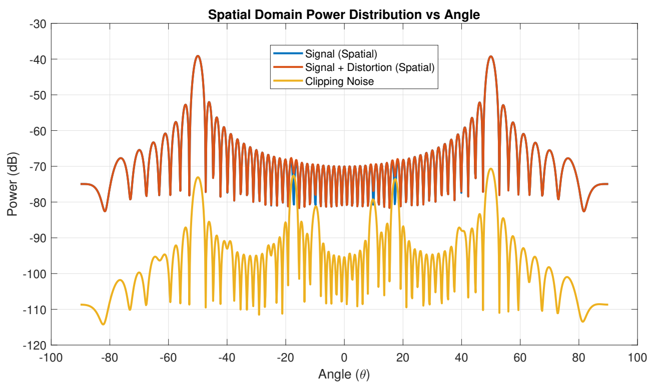

Figure 5.3: Two-user spatial multiplexing with reduced angular separation, e.g. $\theta_1 = -50°$ and $\theta_2 = 50°$. At the considered operating point, the worst-branch EVM is about 2.581%, while user EVMs are approximately 2.195% and 2.186%.

5.1.4 Increasing Number of Users

Finally, the number of simultaneously scheduled users was increased to study how spatial loading and distortion correlation affect EVM. Figure 4.4 shows an example with four users at angles $\{-50°, -30°, 30°, 50°\}$. For the chosen operating point, the worst-branch EVM is about 2.49 %, whereas the user EVMs lie between 1.80 % and 1.91 %.

Compared to the single- and two-user cases, the stronger spatial super position of beams produces a more irregular in-band distortion pattern across the array. The distortion energy is now spread over several angular directions and is therefore less aligned with any individual user beam. Even though the instantaneous PAPR at some branches increases due to multi-user superposition, each user benefits from spatial averaging of the in-band distortion and from the reduced correlation between its beam and the distortion field. As a result, the user EVM remains well below the worst branch EVM, indicating that higher branch distortion can be tolerated without immediately violating the user-level EVM constraint.

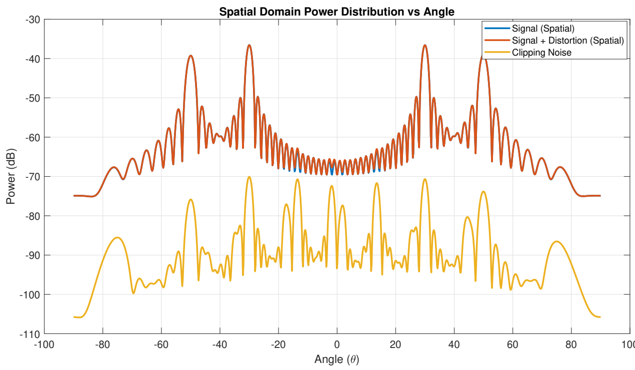

Figure 5.4: Spatial multiplexing with four users at angles $\{-50°, -30°, 30°, 50°\}$. The worst-branch EVM is approximately 2.487 %, while user EVMs are around 1.811 %, 1.901 %, 1.905 %, and 1.799 %.

To further stress the array, eight users were scheduled simultaneously at angles $\{-50°, -41°, -24°, -15°, 10°, 29°, 47°, 55°\}$. As illustrated in Figure 4.5, the resulting radiation pattern exhibits several overlapping main-lobes and an even more uneven distribution of in-band distortion over the branches. At the selected operating point, the worst-branch EVM is still on the order of 2.34 %, but user EVMs drop to between about 1.17 % and 1.26 %.

This result highlights a central insight of the distortion-aware modelling in this thesis. As the number of spatially multiplexed users increases, the distortion observed at individual antenna branches does not directly translate into user EVM. Distortion components generated at different branches combine more non-coherently in the users' directions, while the desired signals remain coherently beamformed. Hence the correlation between each user beam and the in-band distortion field decreases, and the system can tolerate higher branch EVM levels before the user EVM reaches a given target. Although explicit power-overbooking algorithms are not implemented here, the growing gap between branch and user EVM suggests a non-negligible headroom that could be exploited by distortion-aware power allocation in future work.

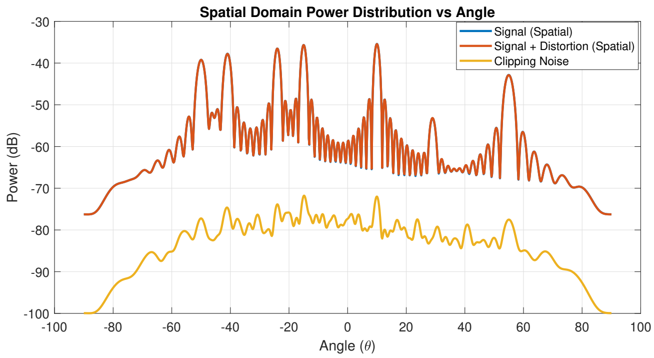

Figure 5.5: Spatial multiplexing with eight users at angles $\{-50°, -41°, -24°, -15°, 10°, 29°, 47°, 55°\}$. The worst-branch EVM is approximately 2.339%, while user EVMs range from about 1.174% to 1.256%.

5.2 Frequency Multiplexing

In frequency multiplexing, users are separated in the frequency domain by assigning disjoint PRB sub-bands within the same 100 MHz carrier, while the spatial layer configuration is kept fixed. This section compares full-band and sub-band allocation and studies how array size and sub-banding affect PAPR, in-band distortion, and the resulting user and branch EVM.

5.2.1 Full-band Allocation and Array Size

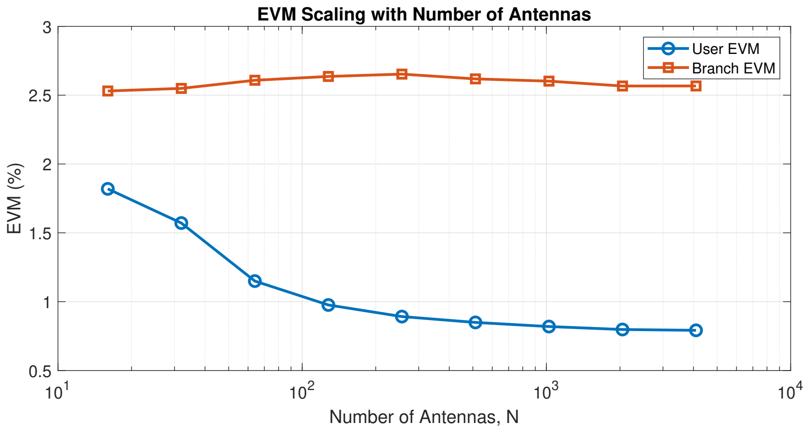

Figure 5.6: Shows a graph of how EVM varies with array size.

In the full-band case, all scheduled users occupy the entire active bandwidth and share the same OFDM resource grid. CFR with iterative clipping and noise filtering is configured to reach a target PAPR of approximately 7.5 dB after four iterations, as described in Section 3.2. The clip-and-filter operation suppresses out-of-band regrowth, leaving only in-band distortion that directly impacts EVM.

For full-band allocation, the branch EVM saturates at approximately 3.5% across all array sizes. This indicates that the CFR operating point is fundamentally constrained by the in-band distortion tolerated by the PA, rather than by the number of antennas. In contrast, the user-beam EVM decreases with increasing N, from approximately 2.3% at $N = 16$ to below 1% at $N = 256$.

This behaviour follows directly from spatial distortion averaging: the desired signal combines coherently across antennas, while the distortion combines non-coherently. Consequently, the effective signal-to-distortion ratio improves with array gain, leading to reduced user EVM.

The growing gap between branch and user EVM implies that larger arrays inherently provide additional margin for distortion-aware transmit power control, even when the CFR operating point remains unchanged.

5.2.2 Sub-band Allocation and Distortion Decorrelation

In the sub-band case, the 100 MHz carrier is partitioned into smaller contiguous PRB groups, and each user (or beam) is assigned a separate sub-band. The CFR parameters are kept identical to the full-band case; hence, any performance differences arise from how sub-banding reshapes the in-band distortion in the time–frequency domain.

Table 5.1: User and branch EVM for full-band and sub-band frequency multiplexing at $N = 16$.

Metric	Sub-band	Full-band
2 beams: user EVM	2.22%	2.49%
2 beams: branch EVM	2.70%	2.73%
4 beams: user EVM	1.96%	2.07%
4 beams: branch EVM	2.69%	2.74%

Sub-band allocation consistently reduces user EVM while leaving branch EVM nearly unchanged, indicating that the total in-band distortion power at the PA output is approximately conserved but redistributed across frequency.

This mechanism follows from spectral orthogonality:

$$\mathcal{B}_k \cap \mathcal{B}_j = \emptyset, \quad k \neq j, \tag{5.1}$$

which suppresses cross-beam distortion coupling:

$$P_{\text{cross}}(k \to j) \approx 0. \tag{5.2}$$

As a result, the clipping distortion becomes less correlated with the desired signal and behaves as approximately uncorrelated interference from each user's perspective. This reduces its projection onto the beamforming direction and directly lowers the user EVM.

5.2.3 EVM CCDF Comparison: Full-band vs. Sub-band

The complementary cumulative distribution function (CCDF) of the EVM is evaluated to characterize the distribution of distortion across both allocation strategies for $N = 16, 64$, and 256. The CCDF provides the probability that the EVM exceeds a given threshold, thereby quantifying system reliability under distortion constraints.

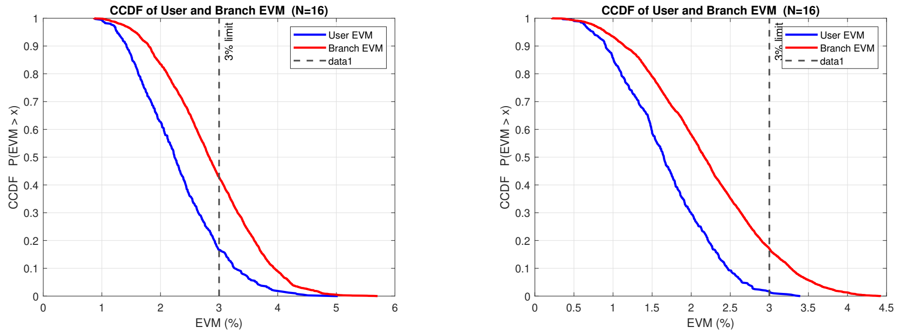

Figure 5.7: EVM CCDF comparison for full-band(left) and sub-band (right) allocation at $N = 16$.

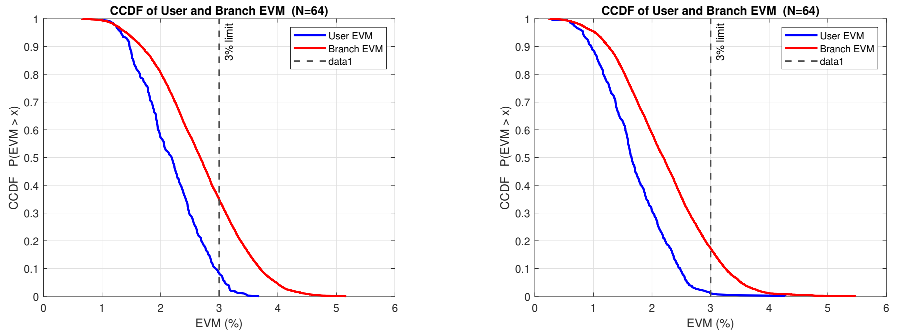

Figure 5.8: EVM CCDF comparison for full-band (left) and sub-band (right) allocation at $N = 64$.

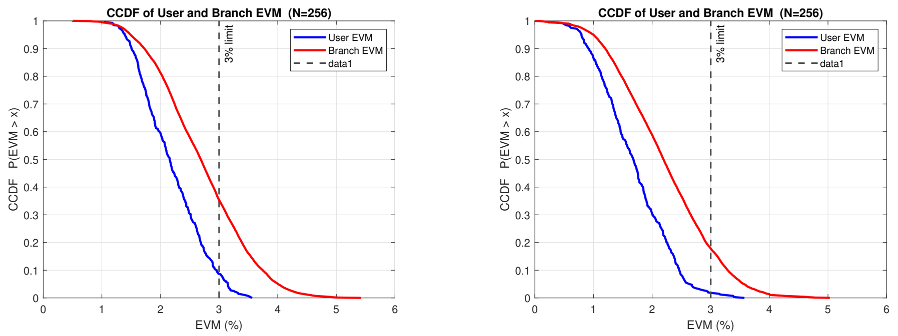

Figure 5.9: EVM CCDF comparison for full-band (left) and sub-band (right) allocation at $N = 256$.

The CCDF results reveal a clear distinction between full-band and sub-band allocation strategies. In the full-band configuration, a significant portion of both beam (user) EVM and branch EVM distributions exceeds the 3% EVM limit, indicating a higher probability of distortion constraint violations. In particular, the branch EVM exhibits a heavier tail, reflecting a greater likelihood of large distortion events.

In contrast, sub-band allocation leads to a noticeable shift of both EVM distributions toward lower values. The probability of exceeding the 3% threshold is significantly reduced for both beam and branch EVM, demonstrating improved compliance with the EVM constraint. This improvement stems from the spectral isolation of clipping noise, which eliminates cross-beam distortion coupling.

Furthermore, at the median probability level (CCDF = 0.5), the separation between the beam and branch EVM curves is larger in the sub-band case compared to the full-band case. This wider separation indicates an increased operating margin, confirming that sub-banding provides a more favorable distortion distribution and enables better system robustness.

Across both allocation strategies, increasing the array size N results in a significant improvement in EVM performance. As N increases, the EVM distributions progressively shift toward lower values, reflecting enhanced spatial orthogonality and improved distortion averaging across antenna elements. This leads to a reduced probability of exceeding the EVM limit for both beam and branch metrics. The improvement is more pronounced in the sub-band configuration, where spatial and frequency-domain isolation jointly contribute to superior distortion suppression.

5.2.4 Power Overbooking with Frequency Multiplexing

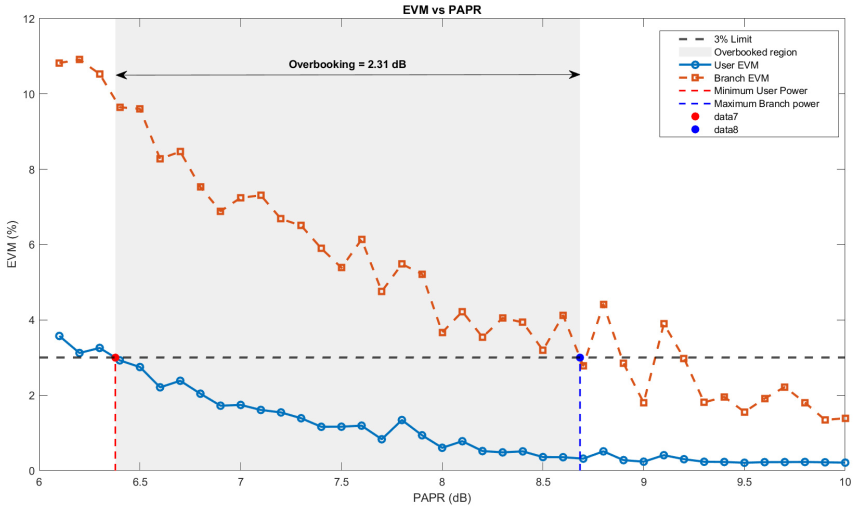

Figure 5.10: Shows how power overbooking is determined.

To quantify the available transmit power margin under nonlinear distortion constraints, EVM-versus-PAPR sweeps are performed. Two critical operating points are defined:

- X: maximum allowable PAPR such that the *branch* EVM $\leq 3\%$,
- Y: maximum allowable PAPR such that the *beam* EVM $\leq 3\%$.

The difference between these operating points,

$$\Omega = X - Y, \tag{5.3}$$

represents the *power overbooking margin*, i.e., the excess back-off that can be tolerated at the branch level while still satisfying the beam-domain EVM constraint. Physically, Ω captures the extent to which distortion becomes less harmful after spatial and/or frequency-domain aggregation.

For $N = 16$, full-band allocation achieves $\Omega \approx 0.50$ dB, whereas sub-band allocation increases the margin to approximately 0.70 dB. As the array size scales to $N = 256$, the sub-band overbooking margin further increases to approximately 0.80 dB, indicating improved distortion averaging with higher spatial degrees of freedom.

A detailed comparison across configurations is summarized in Table 5.2.

Table 5.2: Power overbooking for frequency multiplexing

Configuration	Y (dB)	X (dB)	Ω (dB)
Sub-band, $N = 16$, $K = 4$	6.80	7.40	0.60
Full-band, $N = 16$, $K = 4$	7.00	7.40	0.40
Sub-band, $N = 256$, $K = 4$	6.70	7.50	0.80
Full-band, $N = 256$, $K = 4$	6.80	7.50	0.70

Consistently across both array sizes, sub-band allocation provides a higher overbooking margin than full-band transmission. The observed incremental gain,

$$\Delta_{\text{freq}} \approx 0.1\text{-}0.2 \text{ dB}, \tag{5.4}$$

quantifies the additional distortion suppression enabled by *frequency-domain decorrelation*.

From a signal processing perspective, this gain arises because user signals occupying disjoint sub-bands generate distortion products that are less spectrally aligned. As a result, nonlinear distortion components combine *incoherently* at the beam level, reducing their effective contribution to EVM. This mechanism directly mirrors the spatial distortion averaging effect, but operates across frequency resources instead of antennas.

While Δ_{freq} is smaller than the spatial multiplexing gain, it is systematic and scales favorably with array size, indicating that larger systems benefit more from joint domain separation. When combined with spatial multiplexing over K users, the aggregate distortion reduction can be approximated as

$$\Delta_{\text{dist}}^{(\text{joint})} \approx 10 \log_{10}(K) + \Delta_{\text{freq}}, \tag{5.5}$$

highlighting the additive nature of spatial and frequency-domain decorrelation gains.

In practical PA-limited systems, this additional margin translates directly into higher allowable transmit power or reduced back-off, thereby improving power amplifier efficiency. Consequently, frequency multiplexing serves as a complementary dimension to spatial multiplexing, enabling further exploitation of distortion averaging to relax EVM constraints and increase usable transmit power headroom.

5.3 Spatial+Frequency Multiplexing

5.3.1 Power Overbooking Results

Tables 5.3–5.5 summarize the power overbooking margin Ω (dB) obtained across the full parameter sweep over (K, N) and different EVM targets.

In all configurations, both *spatial multiplexing* (via K simultaneous beams) and *frequency multiplexing* (via sub-band allocation across users) are jointly exploited.

From a resource utilization perspective, the observed gains in Ω arise from two complementary mechanisms:

- **Spatial domain (K beams):** Increasing K distributes the transmit signal over multiple spatial streams. Due to limited spatial correlation, nonlinear distortion combines only partially coherently at the beam level, resulting in a dominant gain scaling approximately as $10 \log_{10}(K)$.
- **Frequency domain (sub-band allocation):** Assigning users to disjoint sub-bands spreads distortion products across frequency, reducing spectral overlap and promoting incoherent combining. This introduces an additional gain Δ_{freq}, typically on the order of 0.1–0.2 dB.

Together, these mechanisms allow higher transmit power before violating the beam EVM constraint, which is captured through the increase in Ω.

EVM = 1.8% (Modulation order=1024):

Table 5.3: Power overbooking Ω (dB) @ EVM = 1.8%

K (beams)	$N = 16$	$N = 64$	$N = 256$
2	0.4	0.6	0.9
4	1.0	1.5	1.6
8	1.5	2.3	**2.7**

At standard EVM requirement for 1024-QAM (as per 3GPP), Ω scales strongly with both K and N. The maximum gain of 2.7 dB at $(K, N) = (8, 256)$ reflects efficient distortion averaging across both spatial and frequency domains.

EVM = 3% (Modulation order=256):

Table 5.4: Power overbooking Ω (dB) @ EVM = 3%

K (beams)	$N = 16$	$N = 64$	$N = 256$
2	0.3	0.9	0.7
4	1.0	1.3	1.4
8	1.3	2.3	**2.7**

At the standard 3% EVM target of 256-QAM (requirement as per 3GPP standard), similar scaling trends persist. The dominant dependence on K confirms that spatial multiplexing drives the majority of the gain, while the consistent improvement at larger N indicates enhanced decorrelation benefits.

EVM = 6% (Modulation order=64):

Table 5.5: Power overbooking Ω (dB) @ EVM = 6%

K (beams)	$N = 16$	$N = 64$	$N = 256$
2	0.4	0.5	0.6
4	1.0	1.4	2.0
8	1.5	2.3	**2.7**

With EVM 6%, a standard requirement for 64-QAM, the same joint spatial–frequency gains remain evident, indicating robustness of the approach across operating regimes.

Cross-table interpretation:

Across all EVM targets, three key observations emerge:

- **Spatial scaling dominance:** Increasing K yields the largest improvements in Ω, confirming that spatial multiplexing is the primary mechanism for distortion averaging.
- **Array gain via N:** Larger arrays improve Ω, especially at higher K, due to finer spatial resolution and reduced inter-user correlation.
- **Frequency-domain contribution:** The consistent uplift beyond pure spatial scaling indicates an additional gain Δ_{freq} due to sub-band allocation, validating the role of frequency-domain decorrelation.

These combined effects can be approximated as

$$\Omega \approx 10 \log_{10}(K) + \Delta_{\text{freq}}(N), \tag{5.6}$$

where Δ_{freq} captures the incremental gain from frequency multiplexing.

Engineering implication: The joint exploitation of spatial (K beams) and frequency (sub-band allocation) resources reshapes nonlinear distortion across orthogonal dimensions. This reduces coherent distortion accumulation at the receiver, thereby enabling increased transmit power while maintaining EVM constraints. In practical systems, this directly translates into reduced PA back-off and improved energy efficiency, particularly in large-scale MIMO deployments.

5.3.2 Observed Trends

Four principal trends emerge from the joint evaluation of spatial and frequency multiplexing:

1. **Beam count K is the dominant driver:** Increasing the number of beams from $K = 2$ to $K = 8$ roughly doubles or triples the overbooking margin across all array sizes and EVM targets. This behaviour is consistent with the spatial distortion spreading mechanism described in (3.26), where the per-beam distortion scales approximately as $1/K$.

2. **Array size N amplifies the gain:** For $K = 8$, the overbooking margin increases from 1.5 dB ($N = 16$) to 2.3 dB ($N = 64$) and up to 2.7 dB ($N = 256$) at EVM = 1.8%. Larger arrays provide higher beamforming gain (approximately 18 dB at $N = 256$ versus 6 dB at $N = 16$) and finer angular resolution, which reduces inter-beam distortion coupling and enhances spatial averaging.

3. **Peak overbooking performance:** The maximum observed overbooking is

$$\Omega = 2.7 \text{ dB} \quad \text{at} \quad K = 8,\ N = 256,\ \text{EVM} = 1.8\%.$$

   This corresponds to operating the PA at a transmit power 2.7 dB higher than what would be allowed under worst-case back-off design. Such a gain is highly significant, translating into measurable improvements in link budget, coverage, or spectral efficiency in practical 5G/6G deployments.

4. **Diminishing sensitivity to EVM at high K:** At $K = 8$ and $N = 64$, an overbooking margin of approximately 2.3 dB is achieved across all EVM targets (1.8%, 3%, and 6%). This convergence indicates that the in-band distortion is sufficiently spread across beams such that the per-beam EVM constraint becomes non-limiting over a wide range of modulation requirements.

Overall, these trends confirm that power overbooking is fundamentally enabled by distortion redistribution across spatial and frequency domains. Increasing K and N enhances spatial decorrelation, while sub-band allocation contributes additional frequency-domain isolation. Together, these mechanisms create substantial EVM-based power headroom that can be systematically exploited to improve PA efficiency and transmit power utilization.

Chapter 6

Conclusion and Future Works

6.1 Conclusion

This work investigated the impact of jointly exploiting spatial and frequency multiplexing on nonlinear distortion behavior and transmit power efficiency in multi-user MIMO systems. By systematically analyzing EVM–PAPR characteristics and introducing the concept of power overbooking margin Ω, the study established a quantitative framework to assess how much additional transmit power can be leveraged under a fixed beam-level EVM constraint.

The results demonstrate that *spatial multiplexing* is the dominant mechanism for distortion mitigation, as increasing the number of simultaneously transmitted beams K enables significant distortion averaging. This effect arises from the partial incoherent combination of nonlinear distortion across spatial channels, leading to an approximate gain scaling of $10\log_{10}(K)$. In parallel, increasing the array size N enhances spatial resolution and reduces inter-user correlation, further strengthening this averaging effect and improving the achievable power overbooking margin.

Complementing this, *frequency multiplexing* via sub-band allocation introduces an additional, systematic improvement. By assigning users to distinct spectral regions, distortion components become less spectrally aligned, resulting in further decorrelation and reduced coherent accumulation at the beam level. Although the associated gain Δ_{freq} is modest (typically 0.1–0.2 dB), it is consistent across all configurations and becomes increasingly relevant as system dimensions scale.

The combined effect of spatial and frequency resource utilization can be interpreted as a two-dimensional distortion averaging process, where nonlinear distortion is redistributed across both space and frequency. This joint mechanism enables a total power overbooking margin of up to 2.7 dB in the evaluated scenarios, confirming that substantial transmit power gains are achievable without violating EVM constraints.

From a practical standpoint, these findings have direct implications for power amplifier (PA) operation in massive MIMO transmitters. The increased overbooking margin translates into reduced required back-off, allowing PAs to operate closer to their saturation region where efficiency is maximized. Consequently, the joint spatial–frequency multiplexing strategy provides a viable pathway to improve energy efficiency in next-generation wireless systems, particularly in large-scale deployments with many antennas and users.

In summary, this thesis establishes that:

- Spatial multiplexing provides the primary distortion mitigation through incoherent combining across beams.
- Frequency multiplexing offers a complementary decorrelation mechanism that enhances distortion suppression.
- The joint exploitation of both domains enables meaningful transmit power gains under realistic EVM constraints.

These insights reinforce the importance of multi-dimensional resource allocation in nonlinear system design and highlight that distortion-aware multiplexing strategies are essential for unlocking the full efficiency potential of future massive MIMO architectures.

6.2 Future Work

Future work could extend this study in several directions:

- **Realistic channels and traffic:** Enrich the simulation environment with standardized wideband channels, user mobility and realistic traffic patterns to assess the robustness of the observed power headroom under dynamic conditions.
- **Link adaptation and scheduling:** Integrate the distortion-aware framework with link adaptation and scheduling, using the derived overbooking maps to guide modulation, coding and power-control decisions in real time.
- **Refined hardware modelling:** Incorporate more detailed hardware models, including PA memory effects, device variability and additional RF impairments, to evaluate whether the same spatial and frequency-domain decorrelation mechanisms remain effective under more realistic assumptions.

- **Experimental validation:** Implement the proposed CFR and beamforming chain on a hardware testbed or software-defined radio platform to validate the simulation results and identify additional practical constraints for 5G/6G base-station implementations.

References

[1] Y. Yang, J. Xu, G. Shi, and C.-X. Wang, *5G Wireless Systems: Simulation and Evaluation Techniques.* in Wireless Networks. Cham: Springer International Publishing, 2018. doi: 10.1007/978-3-319-61869-2.

[2] F. Rinaldi, A. Raschellà, and S. Pizzi, '5G NR system design: a concise survey of key features and capabilities', *Wirel. Netw.*, vol. 27, no. 8, pp. 5173–5188, Nov. 2021, doi: 10.1007/s11276-021-02811-y.

[3] S. Marwaha, P. Kryszkiewicz, and E. A. Jorswieck, 'Energy-Efficient Power Control in Single-User M-MIMO-OFDM System with PA Nonlinearity', Oct. 10, 2025, *arXiv*: arXiv:2510.09232. doi: 10.48550/arXiv.2510.09232.

[4] M. B. Salman, E. Björnson, G. Muzaffer Güvensen, and T. Çiloğlu, 'Nonlinear Distortion Correlation Aware Power Allocation for Massive MIMO Systems', *IEEE Trans. Commun.*, vol. 73, no. 6, pp. 4033–4048, Jun. 2025, doi: 10.1109/TCOMM.2024.3506941.

[5] S. R. Aghdam, S. Jacobsson, U. Gustavsson, G. Durisi, C. Studer, and T. Eriksson, 'Distortion-Aware Linear Precoding for Massive MIMO Downlink Systems with Nonlinear Power Amplifiers', Nov. 14, 2021, *arXiv*: arXiv:2012.13337. doi: 10.48550/arXiv.2012.13337.

[6] B. Liu and S. Pollin, 'Distortion-Aware Power Allocation for Multi-Stream Distributed Massive MIMO System With Nonlinear Power Amplifier', *IEEE Open J. Commun. Soc.*, vol. 5, pp. 1566–1578, 2024, doi: 10.1109/OJCOMS.2024.3373333.

[7] S. Wang, M. Roger, and C. Lelandais-Perrault, 'Impacts of Crest Factor Reduction and Digital Predistortion on Linearity and Power Efficiency of Power Amplifiers', IEEE Trans. Circuits Syst. II Express Briefs, vol. 66, no. 3, pp. 407–411, Mar. 2019, doi: 10.1109/TCSII.2018.2855084.

[8] S. Marwaha, P. Kryszkiewicz, and E. Jorswieck, 'Optimal Distortion-Aware Multi-User Power Allocation for Massive MIMO Networks', Sep. 08, 2025. doi: 10.1109/TWC.2025.3632114.

[9] E. Björnson, J. Hoydis, M. Kountouris, and M. Debbah, 'Massive MIMO Systems with Non-Ideal Hardware: Energy Efficiency, Estimation, and Capacity Limits', *IEEE Trans. Inf. Theory*, vol. 60, no. 11, pp. 7112–7139, Nov. 2014, doi: 10.1109/TIT.2014.2354403.

[10] O. T. Demir and E. Bjornson, 'The Bussgang Decomposition of Nonlinear Systems: Basic Theory and MIMO Extensions [Lecture Notes]', *IEEE Signal Process. Mag.*, vol. 38, no. 1, pp. 131–136, Jan. 2021, doi: 10.1109/MSP.2020.3025538.

[11] S. H. Chukkapalli, R. S. P. Sankar, and S. P. Chepuri, 'Distortion-Aware Transmit Precoding for Integrated Sensing and Communication Systems', *IEEE Wirel. Commun. Lett.*, vol. 14, no. 5, pp. 1336–1340, May 2025, doi: 10.1109/LWC.2025.3541966.

[12] S. Marwaha, P. Kryszkiewicz, and E. Jorswieck, 'Energy-Efficient Resource Allocation for PA Distortion-Aware M-MIMO OFDM System', Oct. 10, 2025, *arXiv*: arXiv:2510.09238. doi: 10.48550/arXiv.2510.09238.

[13] T. Schenk, *RF Imperfections in High-rate Wireless Systems.* Dordrecht: Springer Netherlands, 2008. doi: 10.1007/978-1-4020-6903-1.

[14] C. Mollen, C. Mollen, E. G. Larsson, U. Gustavsson, T. Eriksson, and R. W. Heath, *'Out-of-Band Radiation from Large Antenna Arrays', IEEE Commun. Mag., vol. 56, no. 4, pp. 196–203, Apr. 2018, doi: 10.1109/MCOM.2018.1601063*